Synthesis of Hydroxyapatite Containing some Trace Amounts Elements in Simulated Body Fluids

Xiaojun, Guo*[+]***; Dai, Li***

College of Chemistry & Chemical Engineering, Northwest Normal University, Lanzhou, 730070, P.R. CHINA

ABSTRACT: *Spherical-like hydroxyapatite (HA, $Ca_{10}(PO_4)_6(OH)_2$) particles were prepared by the co-precipitation method in a simulated physiological environment. The effect of calcining temperature, calcining time and the Ca/P ratio of the initial feeding on the morphology and crystallinity of HA were investigated in detail. Interestingly, while the Ca/P ratio of the initial feeding is 1.80, the obtained HA powders calcined at 800 °C for 2 h contain trace amounts of Na and Mg ions, and the (Ca+Na+Mg)/P ratio is equal to 1.66, which is close to the stoichiometric ratio 1.67 of HA. And a better route with shorter reaction time for the synthesis of HA containing trace amounts of Na and Mg elements was acquired.*

KEYWORDS: *Hydroxyapatite; Co-precipitation; Simulated body fluids; Calcining temperature.*

INTRODUCTION

Synthetic hydroxyapatite (HA, general formula $Ca_{10}(PO_4)_6(OH)_2$) is one of the most popular bioceramic materials that has excellent biological properties such as nontoxicity, biochemical tolerance, bioactivity, and biocompatibility. Therefore, HA bioceramics have been widely used in biomaterial engineering, orthopedic application and regenerative medicine for bones [1]. In addition, HA-based composites and coatings have been extensively developed and used for biomedical applications due to the difficult solubility of HA under the physiological temperature and pH conditions [2-5].

Many methods have been applied to prepare HA, such as co-precipitation [6,7], sol-gel process [8,9], solid-state reactions [10], spray pyrolysis [11], combustion synthesis [12], hydrothermal synthesis [13], microemulsion [14] and microwave-assisted method [15]. However, in the conditions of higher pH, temperature, ultra sonication and microwave irradiation, the properties of the as-prepared HA may deviate from biological apatite [16-18]. Due to the lack of trace elements, the degradability and bioactivity of synthetic HA is still to be improved in comparison with biological apatite.

HA provides bioactivity, biocompatibility and an ability to initiate osteogenesis. However, biological apatite is not pure HA, containing a small amount of CO_3^{2-}, Cl^-, Na^+, K^+, Mg^{2+} [19]. Additionally, the apatite-forming ability in Simulated Body Fluids (SBF) is a measure of in vivo bioactivity [20]. Therefore, in order to maintain the properties of HA, it could be a better method to prepare HA in the SBF. Synthetic Body Fluids (SBF) or Simulated Body Fluids (SBF), with ion concentrations nearly consistent with those of the inorganic constituents of human blood plasma, was prepared in compliance with the chemical analysis of human body fluid. In the existing

** To whom correspondence should be addressed.*
+ E-mail: guoxj6906@163.com
1021-9986/2019/1/83-91 9/$/5.09

literature about SBF, the SBF is given by *Kokubo et al* [21] and by *Cüneyt Tas* [22] were widely used by other researchers. Compared to the SBF given by *Cüneyt Tas;* by *Kokubo et al.*, the ion concentrations of the SBF solutions given by *Cüneyt Tas* were more closely with those of 'human blood plasma'. Some researchers reported that SBF could be used as a tool to synthesize apatite-like powders in vitro [23]. *Li* [24] reported that platelet-shaped and needle-like nanocrystalline HA powders could be successfully synthesized in SBF solutions using calcium chlorine and diapotassium hydrogen phosphate as starting materials. But longer reaction time (up to 8 days) is necessary to obtain a stoichiometric apatite structure. Therefore, it is meaningful to explore a better route with shorter reaction time for the synthesis of HA containing trace amounts of Na and Mg elements.

In the present work, spherical-like HA particles containing trace amounts of Na and Mg elements were prepared by co-precipitation method in a simulated physiological environment (in SBF solution with 37℃ and pH 7.40). In addition, the effect of calcining temperature, calcining time and the Ca/P ratio of the initial feeding on the morphology and crystallinity of HA were investigated.

EXPERIMENTAL SECTION

Materials

Sodium chloride (NaCl, ≥99.5%), Sodium bicarbonate ($NaHCO_3$, ≥98.9%), Disodium hydrogen phosphate dodecahydrate ($Na_2HPO_4{\cdot}12H_2O$, ≥99%), Calcium nitrate tetrahydrate ($Ca(NO_3)_2{\cdot}4H_2O$, ≥99%), Diammonium hydrogen phosphate ($(NH_4)_2HPO_4$, ≥99%), Absolute ethyl alcohol (CH_3CH_2OH, ≥99.7%) and Ammonia hydroxide ($NH_3{\cdot}H_2O$, 25%~28%) were purchased from Tianjin Kermel Chemical Reagents Development Center (China). Potassium chloride (KCl, ≥99.5%), Magnesium chlordie (MgCl, ≥98%) and Sodium sulfate anhydrous (Na_2SO_4, ≥99%) were supplied by Yantai Shuangshuang Chem Co. (China). Calcium chloride anhydrous ($CaCl_2$, ≥96%) and Tris(hydroxymethyl)methyl aminomethane ($NH_2C(CH_2OH)_3$, ≥99%) were provided by Shanghai Shanpu Chem Co. (China). All the above reagents used were of analytical reagent grade without further purification.

Synthesis of HA powder

According to Ref. [22], SBF solution was prepared by dissolving NaCl, $NaHCO_3$, KCl, $Na_2HPO_4{\cdot}12H_2O$, $MgCl_2{\cdot}6H_2O$, $CaCl_2$, Na_2SO_4, and $(NH_2C(CH_2OH)_3$ in deionized water. During the preparation of 1 L of SBF solutions, 40 mL of 1 M HCl solution was added to adjust the pH of SBF solutions to 7.40.

Calcium nitrate tetrahydrate ($Ca(NO_3)_2{\cdot}4H_2O$) and diammonium hydrogen phosphate ($(NH_4)_2HPO_4$) were used in the co-precipitation runs as calcium and phosphorus ion sources, respectively. SBF solution was used as solvent and ammonia hydroxide ($NH_3{\cdot}H_2O$) was used to adjust the pH of the reaction system to 7.40 (the pH of human plasma is 7.35~7.45).

According to the stoichiometric ratio of HA (Ca/P =1.67), $Ca(NO_3)_2{\cdot}4H_2O$ and $(NH_4)_2HPO_4$ were dissolved in SBF solutions, respectively. $Ca(NO_3)_2{\cdot}4H_2O$-SBF solutions were placed in a beaker and kept in a 37℃ thermostated water bath, and the $NH_3{\cdot}H_2O$ was added to adjust the pH of solution to 7.40. Then $(NH_4)_2HPO_4$-SBF solutions were slowly dropped into the $Ca(NO_3)_2{\cdot}4H_2O$-SBF solutions while stirring, resulting in white precipitates. During the precipitation process, the pH of the mixture was kept in 7.40 by continuous adding the ammonium hydroxide solution. This precipitated solution was rigorously stirred for 1 h and aged at 37℃ for one night without stirring. Finally, the precipitate was separated from the solution by vacuum filter and washed three times using double distilled water and anhydrous ethanol, respectively, followed by drying in a vacuum drying oven at 80℃ for 6 h. The dried sample was termed as HA-80. In the range of 600 to 1250℃, HA-80 was calcined for 2 h at various temperatures in a muffle furnace under normal air atmosphere. Based on the different calcination temperature, the HA batches were denoted as HA-600, HA-700, HA-800, HA-900, HA-1000, HA-1100 and HA-1250.

Characterization

The thermal behavior of the HA powders was investigated by thermogravimetry/differential thermal analysis (TG-DTA, Model: PE-7, USA) with heating temperature ranging from 20℃ to 1200 °C in air at a heating rate of 10℃ min^{-1}.

The phase purity and crystallinity structures of the HA samples were studied by X-ray power diffraction (XRD, Model: D/max-2400, Rigaku, Japan) at the step size of 0.02 s^{-1} in the 2θ range from 10° to 80°. A Cu K_α tube operated at 40 kV and 150 mA was used

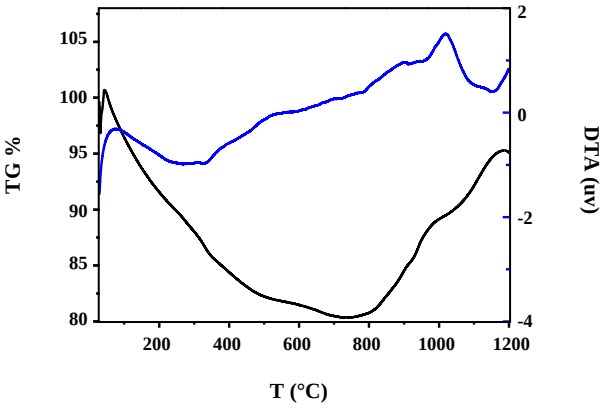

Fig. 1: TG and DTA curves of HA-80 powders.

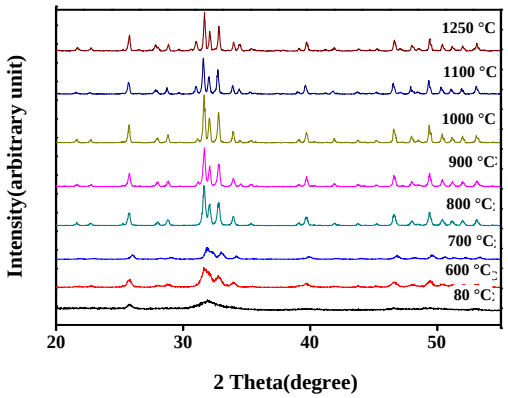

Fig. 2: XRD patterns of 80℃ dried sample and HA samples calcined at different temperature for 2 h.

for the generation of X-rays (λ=1.54178 Å). The crystalline phases were identified with reference to the Joint Committee on Powder Diffraction Standards (JCPDS) files.

The structural characteristics of the HA powders were investigated by Fourier-transform infrared (FTIR, Model: Nicolet 20 DXB spectrophotometer, USA) spectroscopy, and the wave numbers of FTIR were in the range of 4000-400 cm^{-1}.

The morphology of the HA nanoparticles was observed by scanning electron microscope (SEM, Model: ULTRA Plus, Germany), and elemental composition of the HA samples was examined by Energy-dispersive X-ray spectroscopy (EDX).

RESULTS AND DISCUSSION

TG-DTA analysis

The TG-DTA curves of HA-80 particles are shown in Fig. 1. Obviously, there are two weight loss regions before 730 °C from TG curve. The total weight loss of the HA-80 powders is found to be 19.5%. The first weight loss at the range of 45.9-500 °C could be ascribed to desorption of adsorbed water molecules on the crystallite surface and the release of crystalline water. And the second loss at the range of 500-730 °C can be associated with the dehydroxylation and early slow decomposition of HA [25]. Above 730℃, HA decomposition occurs. Interestingly, weight gain is also observed. This shows that when heat-treatment is above 730°C, some new substance may be produced by the reaction of the sample with carbon dioxide from the air. Accordingly, the DTA curve display that there are endothermic and exothermic phenomenon in the heating process.

XRD analysis

The XRD patterns of HA powders calcined at different temperature are shown in Fig. 2. According to Fig. 2, the calcining temperature plays a major role in the formation of HA. It can be seen that HA-80 is an amorphous solid with extremely low crystallinity. When HA-80 powders are calcined at 600 or 700℃, the obtained particles show wider and dispersed peaks owing to the incomplete reaction of diammonium phosphate and calcium nitrate tetrahydrate. The diffraction peaks of HA-800 powders are in good agreement with the standard data of HA (JCPDS No. 09-0432) and no other crystalline phase is present. Furthermore, some key characteristic diffraction peaks of HA can also be observed and corresponding to the (002), (211), (112), (300) and (310) lattice plane, which reveals that the pure phase and homogeneous HA powder is obtained when calcining temperature is 800°C.

From Fig. 2, XRD diffraction patterns of HA-900, HA-1000, HA-1100, and HA-1250 powders contain the main peaks of HA. And these diffraction peaks are intensified gradually, the width of the peaks becomes narrow gradually, which indicated that the crystallinity degree of HA powders was increased with the increase of the calcining temperature.

According to Ref. [26], the crystallinity degree of the samples was calculated as follows:

$$B_{002}\sqrt[3]{X_c} = K \quad (1)$$

Where K is a constant found equal to 0.24, B_{002} is the full width at half maximum of the (002) reflection and X_c is the crystallinity degree.

The calculated values of the crystallinity degree of HA-80, HA-600, HA-700, and HA-800 powders are 0.03, 0.16, 0.39 and 0.80, respectively. Obviously, the crystallinity degree of the samples increased with increasing calcining temperature.

However, as shown in Fig. 2, some miscellaneous peaks were observed at 2θ values of 31.2° and 34.4°, and these peaks were proved to be the major diffraction peaks of β-TCP by XRD analysis software. It could be concluded that HA was decomposed into β-TCP as the calcining temperature increased to 900℃ or above. In addition, the color of HA samples showed a slight purple when the calcining temperature was above 1100 ℃. According to the reported literature [27], we speculated that some samples may react with carbon dioxide in the air under higher temperature conditions and form a small amount of calcium carbide.

The average crystalite size (D) in nm was estimated following the Debye-Scherrer equation [28]:

$$D = \frac{K\lambda}{\beta \cos\theta} \quad (2)$$

Where *K* is the shape factor equal to 0.9, λ is the X-ray wave length (1.541Å), β is the Full Width at Half Maximum (FWHM) in radian and θ is the diffraction angle in degree. The crystallite sizes were calculated for the perpendicular crystal planes (002) and (310), and the calculated values of D_{002} and D_{310} were listed in Table 1. It can be seen that the as-synthesized HA samples have small crystal size. Simultaneously, these data in Table 1 also confirmed that the crystal size of the as-synthesized HA powders increased as the increase of the calcining temperature. The above results indicate that the calcining temperature affected the phase and crystal size of the prepared samples.

What's more, XRD patterns of HA-800 powders at a different calcining time are also displayed in Fig. 3. Obviously, the number of miscellaneous peaks increased with the increase of the calcining time.

According to the above results obtained from XRD analyses, in order to acquire the pure phase and homogeneous HA powders, the optimal calcining temperature is 800°C and the optimal calcining time is 2 h.

FT-IR analysis

The FT-IR spectra of HA powders synthesized under various calcining temperatures were shown in Fig. 4. Three absorption bands were clearly distinguished at 1092, 1041, and 962 cm^{-1} in the ν_3 and ν_1 phosphate mode region. The band at 473 cm^{-1} corresponds to ν_2 bending of the phosphate group. The ν_4 vibrational band of the phosphate groups $(PO_4)^{3-}$ appeared at 570 and 602 cm^{-1} of the FT-IR spectrum. The band at 3571 cm^{-1} corresponds to O-H stretching of the absorbed water and hydroxyl group (OH^-) of HA [29]. The low intensity band at 877 cm^{-1} indicates the acidic phosphate group HPO_4^{2-} due to the P-(OH) stretching vibration. The characteristic band at 632 cm^{-1} can be attributed to structural OH^- groups in the HA lattice. The absorbance bands in the range of 1470-1410 cm^{-1} correspond to ν_3 asymmetrical stretching vibrations of the CO_3^{2-} ions [30]. With the increase of calcining temperature, the absorbed peaks of the CO_3^{2-} ions disappeared gradually as a result of CO_3^{2-} ions converted to CO_2 gas under higher temperature. Although the characteristic bands of HA were observed in all the samples, the intensities of the bands varied among different samples.

SEM observation

The morphology of the HA powders observed by SEM was shown in Fig. 5. On the whole, the size of the samples increased gradually with the increase of calcining temperature. HA-80 powders presented irregular shape and appeared obvious agglomeration. It may be caused primarily by the various processes occurring during the drying of the precursor. Furthermore, it is also possible that the small particles have been embedded in each agglomerated cluster correspond to the calcium nitrate particles, which could be obtained from the recrystallization of the dissolved calcium nitrate during the grind and the subsequent drying process [31]. With the increase of calcination temperature, the morphology of HA samples calcining at different temperature happened a big change. When calcining temperature is equal or greater than 600°C, the obtained powders display nearly uniform structures. Very obviously, a small change in particle size of resulting products has taken place with the increasing of calcining temperature. Especially, the obtained powder calcining at 800°C was spherical-like with clear outline, perfect crystal growth, good dispersion, and uniform particle size. The results agree with the above XRD analysis results. With further increasing of the calcination temperature,

Table 1: Crystal size of the prepared HA samples.

Samples NO.	(002) FWHM	$D_{(002)}$ (nm)	(310)FWHM	$D_{(310)}$ (nm)
HA-80	0.776	10.51	0.400	21.13
HA-600	0.447	18.25	0.447	18.91
HA-700	0.329	24.80	0.4242	19.95
HA-800	0.259	31.49	0.306	27.62
HA-900	0.235	34.70	0.235	35.97
HA-1000	0.212	38.47	0.235	35.97
HA-1100	0.235	34.70	0.235	35.96
HA-1250	0.235	34.70	0.235	35.97

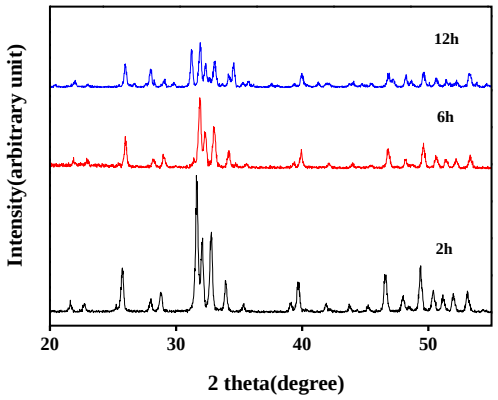

Fig. 3: XRD patterns of HA powders calcined at 800°C with different time.

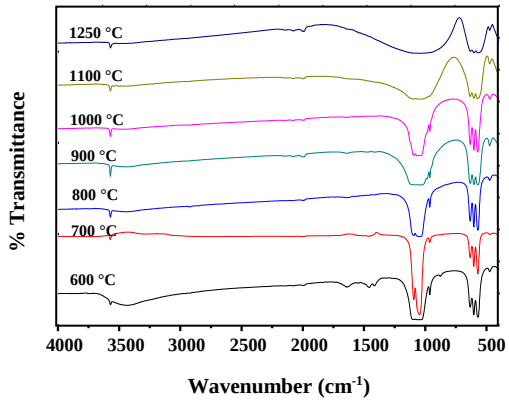

Fig. 4: FT-IR spectra of HA powders calcined at different temperature.

the interparticles forces increase gradually, resulting in the densification of samples gradually as shown in Fig. 5(F), (G) and (H).

EDX analysis

Fig. 6 shows EDX spectra of HA-800 powders. Elemental analysis by EDX confirms that HA-800 powders are primarily composed of Ca, P, and O. Interestingly, 0.24% Na and 0.30% Mg elements were detected in HA-800 powders by EDX. Na and Mg elements originated from the SBF solutions were believed to incorporate themselves in the crystal structure of HA. Some researchers reported that Na^+ and Mg^{2+} ions would replace the Ca^{2+} sites of the HA structure [32]. The calculated (Ca+Na+Mg)/P ratio of HA-800 is 1.60, and this value is less than the stoichiometric ratio of HA (Ca/P =1.67). We speculated that loss of material during the reaction operation process could lead to the above results. In order to clarify the question, the Ca/P ratio of the initial feeding was increased to 1.80 and the other conditions were kept constant, HA-n powders were synthesized following the same method.

Characterization and analysis of HA-n powders

XRD patterns of HA-800 and HA-n powders are compared in Fig. 7. Both spectra showed only reflections associated with HA according to JCPDS No. 09-0432. From the full width at half maximum of the (002) reflection, the crystallinity degree of HA-n powders is higher than HA-800.

The FT-IR spectrum of HA-n powders showed the presence of the characteristic bands of HA (Fig. 8). The bands at 3572 and 632 cm^{-1} were due to the vibrations of OH^-. The bands at 962, 1043 and 1092 cm^{-1} corresponded to P-O stretching vibration, and the bands at 470, 570 and 601 cm^{-1} were the bending vibrations of P-O. The bands at 873, 1418 and 1489 cm^{-1} were assigned to CO_3^{2-}

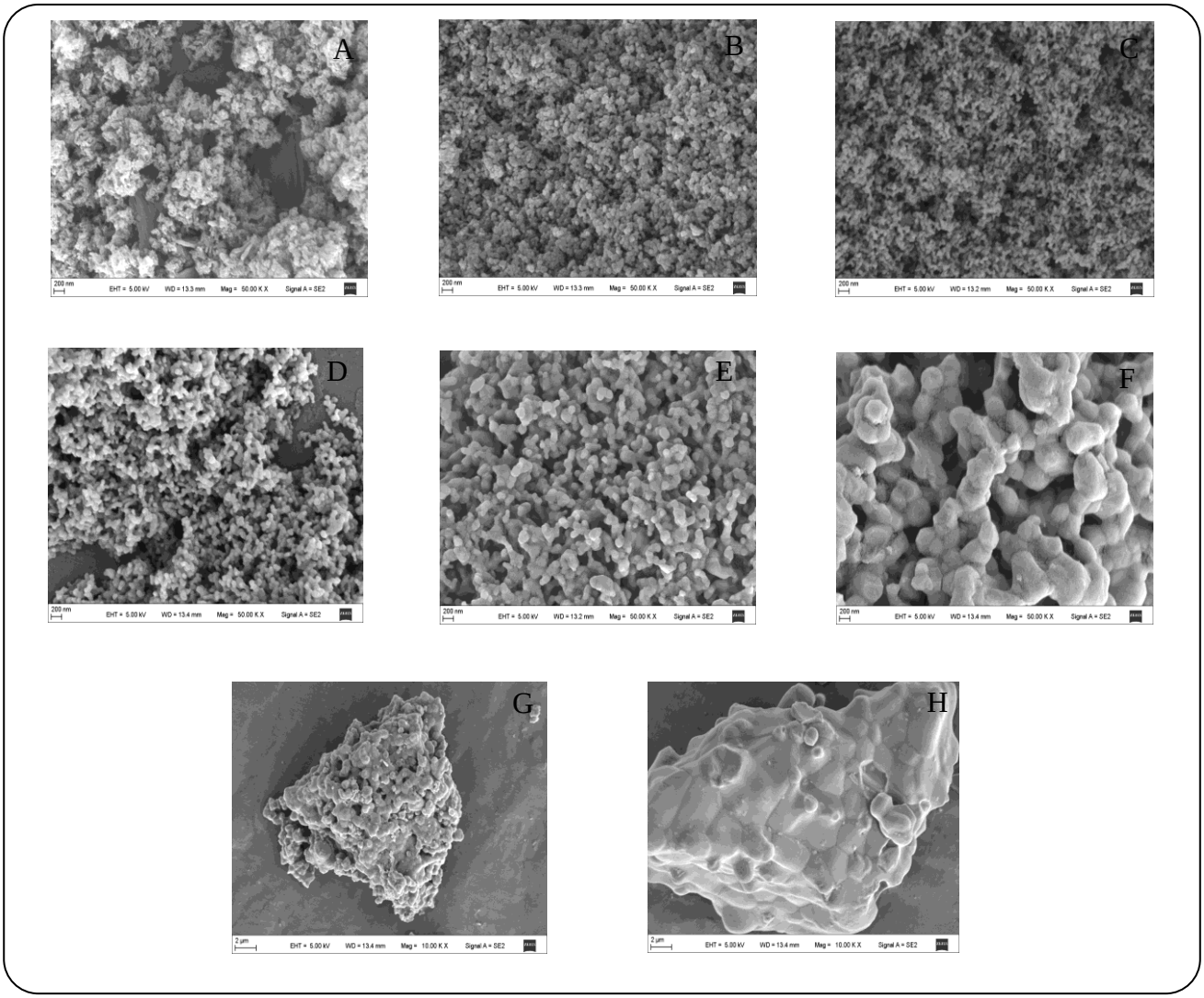

Fig. 5: SEM images of 80 °C dried sample and HA samples calcined at different temperature for 2 h (A: 80 °C, B: 600 °C, C: 700 °C, D: 800 °C, E: 900 °C, F: 1000 °C, G: 1100 °C, H: 1250 °C).

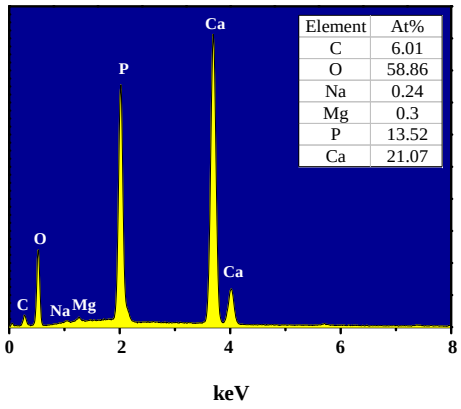

Fig. 6: EDX analysis result of HA-800 powders.

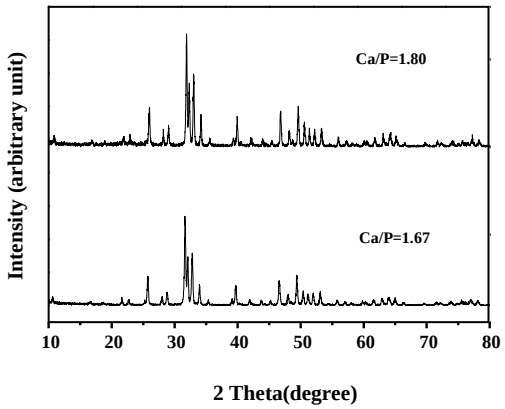

Fig. 7: XRD patterns of HA-n powders and HA-800 powders.

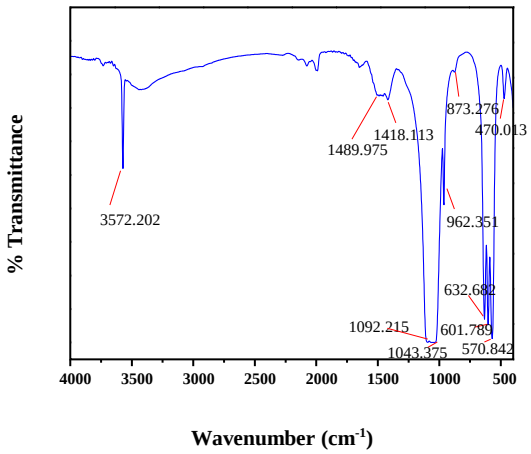

Fig. 8: FT-IR spectra of HA-n powders.

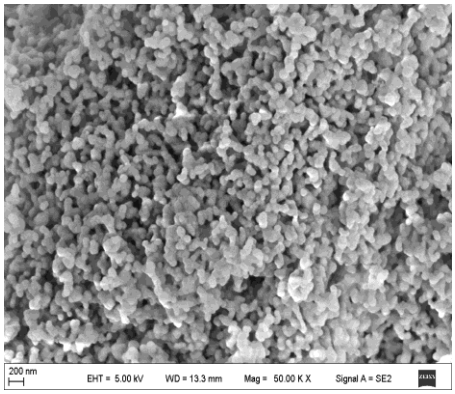

Fig. 9: SEM image of HA-n powders.

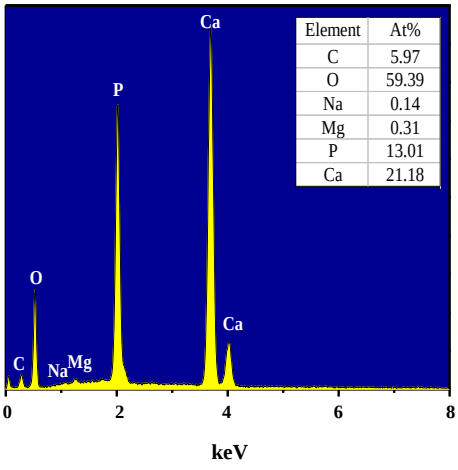

Fig. 10: EDX analysis result of HA-n powders.

in HA-n, which indicated that there might be a possible replacement of PO_4^{3-} or OH^- by CO_3^{2-} in the HA structure.

The morphology of HA-n powders was also investigated by SEM (shown in Fig. 9). A comparison with HA-800 powders (Fig. 7(D)) indicated that HA-n showed a similar spherical-like structure and had clear outline, perfect crystal growth, good dispersion, and uniform particle size.

The results of EDX analysis of HA-n powders were shown in Fig. 10, which revealed that 0.14% Na and 0.31% Mg had been incorporated successfully into the structure of HA. In addition, the calculated (Ca+Na+Mg)/P ratio of HA-800 is 1.66, which is further close to the stoichiometric value of HA (Ca/P =1.67).

CONCLUSIONS

Using calcium nitrate tetrahydrate and diammonium hydrogen phosphate as starting calcium and phosphorous sources, spherical-like HA particles were successfully prepared by the co-precipitation method in SBF solutions. The calcining temperature, calcining time and Ca/P ratio of the initial feeding had an obvious effect on the morphology and crystallinity of the resulting HA samples. While the Ca/P ratio of the initial feeding is 1.80, after calcining at 800°C for 2 h, the obtained HA powders contain trace amounts of Na and Mg ions, and the (Ca+Na+Mg)/P ratio is equal to 1.66, which is close to the stoichiometric ratio 1.67 of HA. In this study, a better route with shorter reaction time for HA containing trace amounts of Na and Mg elements synthesis was proposed. This HA can be used as a biomaterial for various biomedical applications.

Acknowledgements

The work was financially supported by the Fundamental Research Funds for the Universities of Gansu Province and Key Laboratory of Polymer Materials of Gansu Province.

Received : Sep. 16, 2017 ; Accepted : Jan. 15, 2018

REFERENCES

[1] Mossaad C., Tan M.C., Starr M., Andrew Payzant E., Howe J.Y., Riman R.E., Size-dependent Crystalline to Amorphous Uphill Phase Transformation of Hydroxyapatite Nanoparticles, *Cryst. Growth Des.*, **11**:45-52 (2011).

[2] Abdal-hay A., Vanegas P., Hamdy A.S., Engel F.B., Lim J.H., Preparation and Characterization of Vertically Arrayed Hydroxyapatite Nanoplates on Electrospun Nanofibers for Bone Tissue Engineering, *Chem. Eng. J.*, **254**: 612-622 (2014).

[3] Sygnatowicz M., Tiwari A., Controlled Synthesis of Hydroxyaoatite-based Coating for Biomedical Application, *Mater. Sci. Eng., C*, **29**: 1071-1076 (2009).

[4] Sarkar A., Kannan S., In situ Synthesis, Fabrication and Rietveld Refinement of the Hydroxyapatite/titania Composite Coatings on 316 LSS, *Ceram. Int.*, **40**: 6453-6463 (2014).

[5] Yu J.H., Chu X.B., Cai Y.R., Tong P.J., Yao J.M., Preparation and Characterization of Antimicrobial Nano-hydroxyapatite Composites, *Mater. Sci. Eng., C*, **37**: 54-59 (2014).

[6] Inthong S., Tunkasiri T., Eitssayeam S., Pengpat K., Rujijianngul G., Physical Properties and Bioactivity of Nanocrystalline Hydroxyapatite Synthesized by a Co-precipitation Route, *Ceram. Int.*, **39**: 533-536 (2013).

[7] Wang P.P., Li C.H., Gong H.Y., Jiang X.R., Wang H.Q., Li K.X., Effects of Synthesis Conditions on the Morphology of Hydroxyapatite Nanoparticles Produced by Wet Chemical Process, *Powder Technol.*, **203**: 315-321 (2010).

[8] Chen J.D., Wang Y.J., Chen X.F., Ren L., Lai C., He W., Zhang Q.Q., A Simple Sol-gel Technique for Synthesis of Nanostructured Hydroxyapatite, Tricalcium Phosphate and Biphasic Powders, *Mater. Lett.*, **65**: 1923-1926 (2011).

[9] Sanosh K.P., Chu M.C., Balakrishnan A., Kim T.N., Cho S.J., Preparation and Characterization of Nano-hydroxyapatite Powder Using Sol-gol Technique, *Bull. Mater. Sci.*, **32**: 465-470 (2009).

[10] Pramanik S., Agarwal A.K., Rai K.N., Garg A., Development of High Strength Hydroxyapatite by Solid-state-sintering Process, *Ceram. Int.*, **33**: 419-426 (2007).

[11] Suchanek W., Yoshimura M., Processing and Properties Hydroxyapatite-based Biomaterials for Use as Hard Tissue Replacement Implants, *J. Mater. Res.*, **13**: 94-117 (1997).

[12] Sasikumar S., Vijayaraghavan R., Synthesis and Characterization of Bioceramic Calcium Phosphates by Rapid Combustion Synthesis, *J. Mater. Sci. Technol.*, **26**: 1114-1118 (2010).

[13] Manafi S., Rahimipour M.R., Synthesis of Nanocrystalline Hydroxyapatite Nanorods *via* Hydrothermal Conditions, *Chem. Eng. Technol.*, **34**: 972-976 (2011).

[14] Chen B.H., Chen K.I., Ho M.L., Chen H.N., Chen W.C., Wang C.K., Synthesis of Calcium Phosphates and Porous Hydroxyapatite Beads Prepared by Emulsion Method, *Mater. Chem. Phys.*, **113**: 365-371 (2009).

[15] Poinern G.E.J., Ghosh M.K., Ng Y.J., Lssa T.B., An S., Singh P., Defluoridation Behavior of Nanostructured Hydroxyapatite Synthesized through an Ultrasonic and Microwave Combined Technique, *J. Hazard. Mater.*, **185**: 29-37 (2011).

[16] Kalia P., Vizcay-Barrena G., Fan J.P., Warley A., Di Silvio L., Huang J., Nanohydroxyapatite Shape and Its Potential Role in Bone Formation: an Analytical Study, *J. Royal Soc. Interface*, **11**: 20140004 (2014).

[17] Niakan A., Ramesh S., Ganesan P., Tan C.Y., Purbolaksono J., Chandran H., Ramesh S., Teng W.D., Sintering Behaviour of Natural Porous Hydroxyapatite Derived from Bovine Bone, *Ceram. Int.*, **41**:3024-3029 (2015).

[18] Poinern G.E.J., Brundavanam R.K., Thi Le X., Nicholls P.K., Cake M.A., Fawcett D., The Synthesis, Characterisation and *in vivo* Study of a Bioceramic for Potential Tissue Regeneration Applications, *Sci. Rep.*, **4**:6235 (2014).

[19] Wang Y.J., "Biomedical Ceramic Materials", South China University of Technology Press, Guangzhou (2010).

[20] Lee D.Y., Park J.H., Oh K.T., Lee Y.K., Kim K.M., Kim K.N., Bioactivity of Calcium Phosphate Coatings Prepared by Electrodeposition in a Modified Simulated Body Fluid, *Mater. Lett.*, **60**: 2573-2577 (2006).

[21] Li P.J., Nakanishi K., Kokubo T., de Groot K., Induction and Morphology of Hydroxyapatite, Precipitated from Metastable Simulated Body Fluids on Sol-gel Prepared Silica, *Biomaterials*, **14**: 963-968 (1993).

[22] Cüneyt Tas A., Synthesis of Biomimetic Ca-hydroxyapatite Powders at 37°C in Synthetic Body Fluids, *Biomaterials*, **21**: 1429-1438 (2000).

[23] Greish Y.E., Brown P.W., Phase Evolution during the Formation of Stoichiometric Hydroxyapatite at 37.4°C, *J. Biomed. Mater. Res., Part B: Appl. Biomater.*, **67**: 632-637 (2003).

[24] Li M.S., Lu Y.P., Ge S.S., Synthesis of Nanocrystalline Hydroxyapatite Powders in Simulated Body Fluid, *J. Mater. Sci.*, **40**: 2073-2076 (2005).

[25] Eraković S., Janković A., Veljović D.j., Palcevskis E., Mitrić M., Stevanović T., Janaćković D.j., Mišković-Stanković V., The Corrosion Stability and Bioactivity in Simulated Body Fluid of Silver/hydroxyapatite and Silver/hydroxyapatite/lignin Coatings on Titanium Obtained by Electrophoretic Deposition, *J. Phys. Chem. B*, **117**(6):1633-1643 (2013).

[26] Bianco A., Cacciotti I., Lombardi M., Montanaro L., Bemporad E., Sebastiani M., F-substituted Hydroxyapatite Nanopowders: Thermal Stability, Sintering Behaviour and Mechanical Properties, *Ceram. Int.*, **36**:313-322 (2010).

[27] Li G.D., "Fundamental Study on a Novel Technology of CaC_2 Production from Fine Coke and Fine CaO", Beijing University of Chemical Technology (2011).

[28] Kaygili O., Dorozhkin S.V., Keser S., Synthesis and Characterization of Ce-substituted Hydroxyapatite by Sol-gel Method, *Mater. Sci. Eng., C*, **42**: 78-82 (2014).

[29] Kulanthaivel S., Roy B., Agarwal T., Giri S., Pramanik K., Pal K., Ray S.S., Maiti T.K., Banerjee I., Cobalt Doped Proangiogenic Hydroxyapatite for Bone Tissue Engineering Application, *Mater. Sci. Eng., C*, **58**: 648-658 (2016).

[30] Janković A., Eraković S., Mitrić M., Matić I.Z., Juranić Z.D., Tsui G.C.P., Tang C.Y., Mišković-Stanković V., Rhee K.Y, Park S.J., Bioactive Hydroxyapatite/graphene Composite Coating and Its Corrosion Stability in Simulated Body Fluid, *J. Alloys Compd.*, **624**: 148-157 (2015).

[31] Guo X.J., Yan H.D., Zhao S.G., Zhang L., Li Y.T., Liang X.H., Effect of Calcining Temperature on Particle Size of Hydroxyapatite Synthesized by Solid-state Reaction at Room Temperature, *Adv. Powder Technol.*, **24**: 1034-1038 (2013).

[32] Hench L.L., Wilson J., "An Introduction to Bioceramics", World Scientific, London (1993).